PHYSICAL REVIEW D **94,** 112006 (2016)

Measurement of the $e^+e^- \to K^+K^-$ cross section in the energy range $\sqrt{s} = 1.05 - 2.0$ GeV

M. N. Achasov,[1,2] V. M. Aulchenko,[1,2] A. Yu. Barnyakov,[1,2] M. Yu. Barnyakov,[1,2] K. I. Beloborodov,[1,2,*] A. V. Berdyugin,[1,2] D. E. Berkaev,[1,2] A. G. Bogdanchikov,[1] A. A. Botov,[1] A. R. Buzykaev,[1,2] T. V. Dimova,[1,2] V. P. Druzhinin,[1,2] V. B. Golubev,[1,2] L. V. Kardapoltsev,[1,2] A. G. Kharlamov,[1,2] S. A. Kononov,[1,2] I. A. Koop,[1,2,3] A. A. Korol,[1,2] S. V. Koshuba,[1] D. P. Kovrizhin,[1,2] E. A. Kravchenko,[1,2] A. S. Kupich,[1] A. P. Lysenko,[1] K. A. Martin,[1] A. E. Obrazovsky,[1] A. P. Onuchin,[1,2,3] A. V. Otboyev,[1] E. V. Pakhtusova,[1] E. A. Perevedentsev,[1,2] Yu. A. Rogovsky,[1,2] S. I. Serednyakov,[1,2] Yu. M. Shatunov,[1,2] P. Yu. Shatunov,[1,2] D. A. Shtol,[1,2] Z. K. Silagadze,[1,2] A. N. Skrinsky,[1] I. K. Surin,[1,2] Yu. A. Tikhonov,[1,2] Yu. V. Usov,[1,2] A. V. Vasiljev,[1,2] and I. M. Zemlyansky[1,2]

[1]*Budker Institute of Nuclear Physics, 630090 Novosibirsk, Russia*
[2]*Novosibirsk State University, 630090 Novosibirsk, Russia*
[3]*Novosibirsk State Technical University, 630092 Novosibirsk, Russia*

(Received 1 September 2016; revised manuscript received 18 November 2016; published 9 December 2016)

The $e^+e^- \to K^+K^-$ cross section is measured in the center-of-mass energy range 1.05–2.00 GeV at the SND detector. The measurement is based on data with an integrated luminosity of 35 pb^{-1} collected at the VEPP-2000 e^+e^--collider. The obtained results are consistent with the previous most accurate data obtained in the *BABAR* experiment and have a comparable accuracy.

DOI: 10.1103/PhysRevD.94.112006

I. INTRODUCTION

In this paper, we continue the study of e^+e^--annihilation into kaon pairs with the SND detector begun in experiments at the VEPP-2M collider [1–3]. Data collected with the upgraded SND detector [4–7] in experiments at the VEPP-2000 collider [8] allow us to extend the energy range under study up to 2 GeV and improve the accuracy of cross section measurements.

One of the goals of the experiments at VEPP-2000 is the measurement of the total cross section of e^+e^--annihilation into hadrons necessary for the Standard Model calculation of the muon anomalous magnetic moment and the running electromagnetic coupling. The process $e^+e^- \to K^+K^-$ studied in this work gives a significant contribution to the total hadronic cross section in the center-of-mass (c.m.) energy range $\sqrt{s} = 1$–2 GeV.

The combined analysis of the $e^+e^- \to K^+K^-$ and $e^+e^- \to K_SK_L$ cross sections and the spectral function in the $\tau^- \to K^-K^0\nu_\tau$ decay allows us to test the conserved-vector-current hypothesis, as well as to separate isovector and isoscalar parts of the $\gamma^* \to K\bar{K}$ amplitude. The latter is needed, in particular, to measure the branching fractions for the decays of excited vector states of the ρ, ω, ϕ families to kaon pairs.

The process $e^+e^- \to K^+K^-$ at energies above the ϕ-meson resonance was studied in the OLYA [9], DM1 [10], DM2 [11], SND@VEPP-2M [1], and *BABAR* [12] experiments. The most accurate measurement to date was performed by *BABAR* using the initial-state-radiation technique. It should be noted that there are significant differences between the SND@VEPP-2M and *BABAR* measurements at $\sqrt{s} < 1.4$ GeV, and between the DM2 and *BABAR* measurements at $\sqrt{s} = 1.33$–1.64 GeV [12]. In this paper, the $e^+e^- \to K^+K^-$ cross section is measured in the energy range $\sqrt{s} = 1.05$–2.00 GeV with an accuracy not worse than that in the *BABAR* experiment.

The $e^+e^- \to K^+K^-$ study is also useful from the methodical point of view. The charged kaon identification in the upgraded SND detector is based on information from the threshold aerogel Cherenkov counters [6]. The present analysis is the first work using this identification system and demonstrates its ability to select events with charged kaons.

II. DETECTOR AND EXPERIMENT

SND is an universal nonmagnetic detector collecting data at the VEPP-2000 e^+e^- collider. The main part of the detector is a three-layer electromagnetic calorimeter [4] consisting of 1640 NaI(Tl) crystals. The total thickness of the calorimeter is 13.4 radiation lengths. Its energy resolution for photons is $\sigma_E/E = 4.2\%/\sqrt{4}E(\mathrm{GeV})$, and the angular resolution is σ_ϕ, $\sigma_\theta \simeq 1.5°$. The solid-angle coverage of the calorimeter is about 95% of the 4π. Inside the calorimeter, a nine-layer drift chamber [5] is installed, which is used for measurement of directions and production points of charged particles. Charged particle identification is based on information from the system of threshold aerogel Cherenkov counters (ACC) [6]. It consists of nine counters, which form a cylinder located directly behind the drift chamber. The thickness of the aerogel is about 30 mm. The counters cover the polar angle

*K.I.Beloborodov@inp.nsk.su

range $50° < \theta < 132°$. The Cherenkov light is collected using wavelength shifters located inside the aerogel radiator. In the data analysis, the coordinates of the particle entrance to ACC are calculated. Information from ACC is used only if the particle track extrapolates to the ACC active area that excludes the regions of shifters and gaps between counters. The active area is 81% of the ACC area. There are two ACC options, with a refractive index of 1.05 and 1.13. At energies above the threshold of kaons production ACC with the higher refractive index is used, and a kaon is identified by the requirement of no Cherenkov signal in ACC. For pions, the threshold momentum is about 265 MeV/c.

In this paper, data with an integrated luminosity of 34.6 pb^{-1} are analyzed, which were recorded in several scans of the c.m. energy interval from 1.05 to 2.00 GeV in 2011 and 2012.

During the experiments, the beam energy was monitored using measurements of the magnetic field in the collider bending magnets. For absolute calibration of the collider energy, a scan of the $\phi(1020)$ resonance and its mass measurement were performed. In 2012, the energy was measured in several energy points near 2 GeV using the backscattering-laser-light system [13]. The absolute energy measurements were used to calibrate the momentum measurement in the CMD-3 detector, which collected data at VEPP-2000 in parallel with SND. The c.m. energies for all scan points were then determined with an accuracy of 2–6 MeV using average momentum of Bhabha and $e^+e^- \to p\bar{p}$ events [14,15].

III. SELECTION OF $e^+e^- \to K^+K^-$ EVENTS

The $e^+e^- \to K^+K^-$ events are detected as a pair of back-to-back (collinear) charged particles. Events may contain extra charged tracks originating from δ electrons or beam background, and spurious photons originating from beam background and kaon nuclear interaction in the calorimeter. We select events with at least two reconstructed charged particles. Two of them with the highest energy deposition in the calorimeter must satisfy the following requirements:

(i) the distance between the track and the beam axis $|d_i| < 0.25$ cm;
(ii) the difference between z coordinates of the interaction point and the point at the track closest to the beam axis $|z_i| < 7$ cm;
(iii) $|z_1 - z_2| < 1$ cm;
(iv) $|\Delta\phi| < 10°$ for $\sqrt{s} < 1.09$ GeV, $|\Delta\phi| < 5°$ for $1.09 < \sqrt{s} < 1.20$ GeV, $|\Delta\phi| < 3°$ for $\sqrt{s} > 1.2$ GeV, where $\Delta\phi = |\phi_1 - \phi_2| - 180°$, and ϕ_i is the track azimuthal angle;
(v) $|\Delta\theta| < 10°$ for $\sqrt{s} < 1.2$ GeV, $|\Delta\theta| < 7°$ for $\sqrt{s} > 1.2$ GeV, where $\Delta\theta = \theta_1 + \theta_2 - 180°$, and θ_i is the track polar angle;
(vi) one of the particles extrapolates to the ACC active area and does not produce any signal in ACC.

At $\sqrt{s} < 1.2$ GeV, a significant suppression of background processes with electrons, muons, and pions in the final state can be achieved using ionization energy loss (dE/dx) measurements in the drift chamber. The following condition on the sum of dE/dx of two particles is applied: $(dE/dx)_1 + (dE/dx)_2 > k(dE/dx)_e$, where $(dE/dx)_e$ is the average dE/dx for electrons, and the coefficient k is equal to 3 for $\sqrt{s} < 1.1$, and 2.5 for $1.1 < \sqrt{s} < 1.2$ GeV.

At $\sqrt{s} > 1.9$ GeV, it is required that dE/dx of one of the charged particles do not exceed $1.5(dE/dx)_e$. This condition is used to suppress the background from $e^+e^- \to p\bar{p}$ events.

IV. BACKGROUND SUBTRACTION

Background events can be divided into two groups, collinear and noncollinear. The first group includes two-body processes $e^+e^- \to e^+e^-$, $\mu^+\mu^-$, $\pi^+\pi^-$, and $p\bar{p}$, as well as events with cosmic muons passing near the interaction point. The second group contains mainly multibody processes with two charged particles: $e^+e^- \to \pi^+\pi^-\pi^0$, $\pi^+\pi^-\pi^0\pi^0$, $K^+K^-\pi^0$, etc. The process $e^+e^- \to \phi\gamma \to K^+K^-\gamma$, where the photon is emitted from the initial state, also contributes to the second group. This process is strongly suppressed by the condition on $\Delta\theta$. Its contribution is significant only near ϕ-meson resonance, at $\sqrt{s} < 1.06$ GeV, and in the narrow region $1.75 < \sqrt{s} < 1.80$ GeV, where the $e^+e^- \to K^+K^-\gamma$ cross section is very small.

The background subtraction is performed in two stages. At the first stage, the number of background noncollinear events is determined. The collinear background is subtracted at the second stage.

A. Noncollinear background

The noncollinear background is estimated from the two-dimensional distribution of $\Delta\phi$ and $\Delta\theta$. Such a distribution for selected data events from the energy range $\sqrt{s} =$ 1.4–1.6 GeV is shown in Fig. 1. The dashed lines indicate the boundaries of the conditions on $\Delta\phi$ and $\Delta\theta$. The central box in the plot is a signal region corresponding to the standard selection criteria for $e^+e^- \to K^+K^-$ candidates. The peak of signal and background collinear processes is clearly seen in the center of the signal region. Noncollinear processes is expected to have a flat $\Delta\phi$ vs $\Delta\theta$ distribution. The number of noncollinear background events in the signal region ($n_{\rm bkg}$) is estimated from the number of events in four regions located in the corners of the two-dimensional plot ($n'_{\rm bkg}$) as $n_{\rm bkg} = \alpha_{\rm bkg} n'_{\rm bkg}$. The value of the $\alpha_{\rm bkg}$ coefficient is estimated from Monte Carlo (MC) simulation of the main noncollinear background processes $e^+e^- \to 3\pi$, $e^+e^- \to 4\pi$, $e^+e^- \to K^+K^-\pi^0$, $e^+e^- \to K^+K^-\eta$ and found to be equal to unity with 10% uncertainty. Figure 2 shows the distribution of the normalized total energy deposition in the calorimeter $E_{\rm tot}/\sqrt{s}$ for data

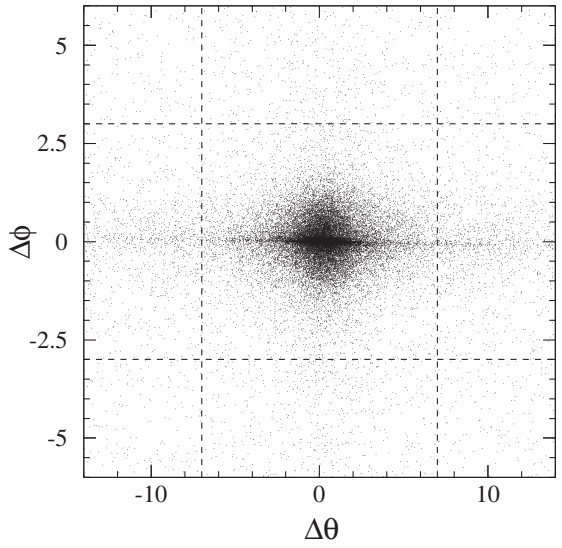

FIG. 1. The two-dimensional $\Delta\phi$ vs $\Delta\theta$ distribution for selected data events with $\sqrt{s} = 1.4$–1.6 GeV. The dashed lines indicate the boundaries of the conditions on $\Delta\phi$ and $\Delta\theta$. The central box is a signal region corresponding to the standard selection criteria for $e^+e^- \to K^+K^-$ candidates.

events from the signal region. The shaded histogram shows the contribution of noncollinear background events estimated using the procedure described above. In further analysis, the noncollinear background is subtracted from the number of events in the signal region. Its fraction

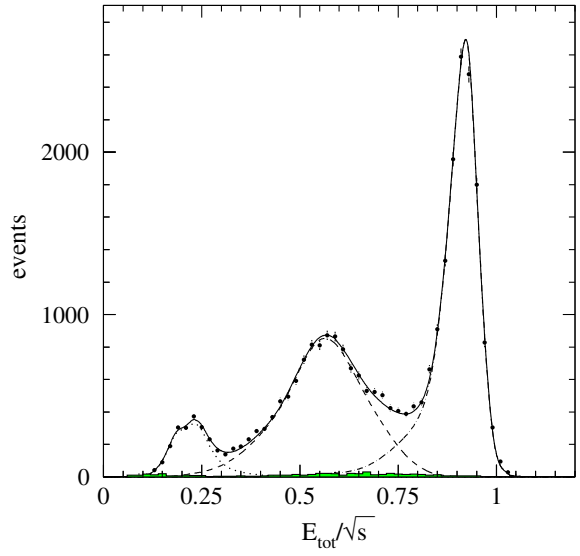

FIG. 2. The distribution of the normalized total energy deposition in the calorimeter for selected data events with $\sqrt{s} = 1.4$–1.6 GeV (points with error bars). The shaded histogram represents the noncollinear background. The dotted, dashed, and dash-dotted curves show the contribution of $e^+e^- \to \mu^+\mu^-$ and cosmic events, $e^+e^- \to K^+K^-$ events, and $e^+e^- \to e^+e^-$ events, respectively. The solid curve is the sum of these three components.

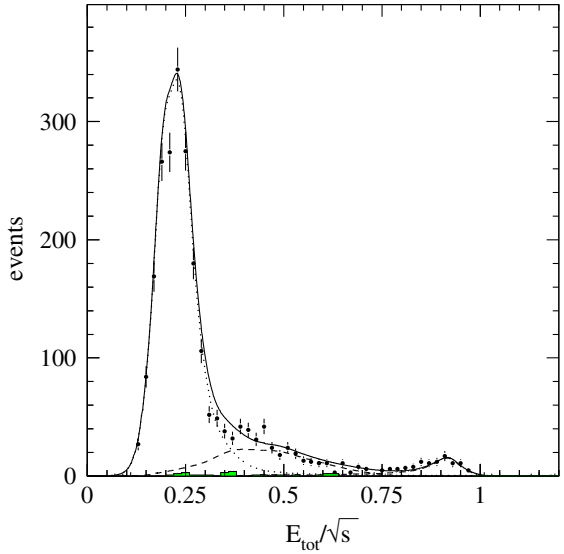

FIG. 3. The distribution of the normalized total energy deposition in the calorimeter for data events with $\sqrt{s} = 1.4$–1.6 GeV selected with the additional requirement that the muon system fires (points with error bars). The shaded histogram represents the noncollinear background. The descriptions of the curves are given in the caption of Fig. 2.

changes slowly from 3% at 1.1 GeV to 5% at 1.65 GeV, and then increases up to 40% at $\sqrt{s} > 1.8$ GeV.

B. Collinear background

The contributions of the process under study (middle peak) and background processes, $e^+e^- \to \mu^+\mu^-$ plus

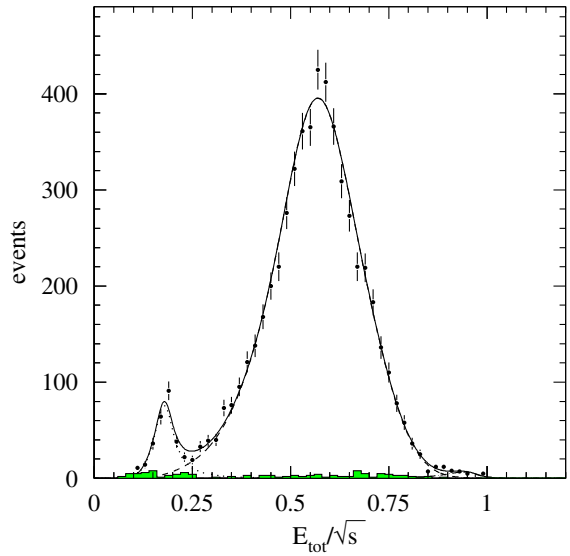

FIG. 4. The distribution of the normalized total energy deposition in the calorimeter for data events with $\sqrt{s} = 1.4$–1.6 GeV in which the condition of no ACC signal is applied to both particles (points with error bars). The shaded histogram represents the noncollinear background. The descriptions of the curves are given in the caption of Fig. 2.

cosmic muons (left peak) and $e^+e^- \to e^+e^-$ (right peak), are clearly seen in the $E_{\rm tot}/\sqrt{s}$ distribution shown in Fig. 2. It should be noted that the requirement of no ACC signal for one of the charged particles suppresses $e^+e^- \to e^+e^-$ and $e^+e^- \to \mu^+\mu^-$ events by a factor of about 300. Background from the $e^+e^- \to p\bar{p}$ process is completely rejected by the selection criteria used, in particular, the requirement on dE/dx.

The $E_{\rm tot}/\sqrt{s}$ distribution for $e^+e^- \to \pi^+\pi^-$ events is close to that for kaons. Their fraction under the kaon peak calculated using MC simulation decreases from 5% at 1.2 GeV to 0.1% at $\sqrt{s} = 1.6$ GeV, and then increases reaching about 8% at 1.8 GeV. The calculation uses the $e^+e^- \to \pi^+\pi^-$ cross section measured in Ref. [16].

The accuracy of the $e^+e^- \to \pi^+\pi^-$ simulation and, in particular, the probability for a pion to not produce a signal in ACC are tested in the energy range $1.05 \geq \sqrt{s} \leq 1.15$ GeV, where the cross section of this process is relatively high. The standard criteria are applied to select $e^+e^- \to \pi^+\pi^-$ events, except the condition on (dE/dx),

TABLE I. Data for the 2011 scan. The c.m. energy ($\sqrt{s}$), integrated luminosity (L), number of selected $e^+e^- \to K^+K^-$ events ($N_{\rm exp}$), detection efficiency (ε_0), radiative correction factor $(1+\delta)$, and $e^+e^- \to K^+K^-$ Born cross section (σ_0). For the number of events, only the statistical uncertainty is quoted. For the cross section, the first error is statistical, the second is systematic. The value in parentheses is a part of the systematic uncertainty associated with background subtraction.

$\sqrt{s}$, GeV	L, nb^{-1}	$N_{\rm exp}$	ε_0	$1+\delta$	σ_0, nb
1.047	426	3975 ± 63	0.229	1.126	$36.243 \pm 0.592 \pm 0.471(0.000)$
1.075	566	3744 ± 61	0.400	0.895	$18.483 \pm 0.305 \pm 0.240(0.000)$
1.097	568	3436 ± 59	0.487	0.876	$14.184 \pm 0.244 \pm 0.184(0.000)$
1.124	550	3292 ± 58	0.594	0.890	$11.307 \pm 0.199 \pm 0.147(0.000)$
1.151	499	2460 ± 50	0.584	0.896	$9.415 \pm 0.192 \pm 0.122(0.000)$
1.174	557	2917 ± 54	0.638	0.898	$9.148 \pm 0.171 \pm 0.119(0.000)$
1.196	566	2441 ± 48	0.618	0.903	$7.737 \pm 0.153 \pm 0.101(0.000)$
1.223	575	2350 ± 56	0.639	0.880	$7.269 \pm 0.175 \pm 0.104(0.042)$
1.245	480	1747 ± 49	0.624	0.879	$6.624 \pm 0.187 \pm 0.092(0.033)$
1.273	513	1928 ± 50	0.654	0.881	$6.518 \pm 0.170 \pm 0.089(0.029)$
1.295	497	1680 ± 52	0.643	0.881	$5.964 \pm 0.184 \pm 0.081(0.023)$
1.323	565	1900 ± 51	0.666	0.883	$5.718 \pm 0.154 \pm 0.077(0.020)$
1.344	598	1801 ± 52	0.660	0.885	$5.160 \pm 0.148 \pm 0.069(0.017)$
1.374	626	1971 ± 49	0.668	0.888	$5.308 \pm 0.132 \pm 0.072(0.022)$
1.394	624	1834 ± 48	0.661	0.889	$5.001 \pm 0.131 \pm 0.067(0.015)$
1.423	588	1646 ± 43	0.683	0.891	$4.579 \pm 0.121 \pm 0.063(0.019)$
1.443	473	1200 ± 39	0.668	0.893	$4.254 \pm 0.137 \pm 0.057(0.014)$
1.471	620	1551 ± 42	0.686	0.891	$4.093 \pm 0.111 \pm 0.056(0.018)$
1.494	754	1648 ± 50	0.672	0.892	$3.646 \pm 0.110 \pm 0.049(0.014)$
1.522	508	1138 ± 38	0.684	0.889	$3.679 \pm 0.124 \pm 0.050(0.015)$
1.543	578	1159 ± 42	0.668	0.889	$3.382 \pm 0.122 \pm 0.045(0.009)$
1.572	533	1140 ± 39	0.684	0.889	$3.518 \pm 0.121 \pm 0.048(0.015)$
1.594	462	959 ± 41	0.667	0.888	$3.507 \pm 0.152 \pm 0.047(0.013)$
1.623	545	1010 ± 34	0.684	0.898	$3.022 \pm 0.102 \pm 0.043(0.018)$
1.643	499	846 ± 32	0.662	0.911	$2.815 \pm 0.106 \pm 0.039(0.012)$
1.669	483	663 ± 28	0.679	0.937	$2.155 \pm 0.091 \pm 0.031(0.012)$
1.693	490	494 ± 25	0.668	0.956	$1.570 \pm 0.081 \pm 0.023(0.011)$
1.723	539	349 ± 25	0.682	0.976	$0.968 \pm 0.069 \pm 0.020(0.016)$
1.742	529	224 ± 18	0.662	1.014	$0.633 \pm 0.051 \pm 0.013(0.010)$
1.774	485	111 ± 13	0.683	1.100	$0.310 \pm 0.036 \pm 0.009(0.009)$
1.793	412	50 ± 10	0.667	1.084	$0.170 \pm 0.035 \pm 0.008(0.008)$
1.826	529	74 ± 12	0.685	0.957	$0.215 \pm 0.034 \pm 0.012(0.011)$
1.849	438	44 ± 10	0.654	0.895	$0.171 \pm 0.038 \pm 0.020(0.020)$
1.871	669	116 ± 15	0.683	0.871	$0.291 \pm 0.036 \pm 0.017(0.016)$
1.893	624	125 ± 15	0.668	0.867	$0.345 \pm 0.040 \pm 0.016(0.016)$
1.901	494	96 ± 14	0.650	0.867	$0.343 \pm 0.049 \pm 0.013(0.013)$
1.927	626	111 ± 15	0.644	0.872	$0.316 \pm 0.042 \pm 0.014(0.014)$
1.953	330	66 ± 11	0.637	0.878	$0.357 \pm 0.061 \pm 0.015(0.014)$
1.978	449	85 ± 14	0.642	0.886	$0.332 \pm 0.055 \pm 0.017(0.017)$
2.005	582	122 ± 16	0.641	0.893	$0.367 \pm 0.048 \pm 0.016(0.015)$

TABLE II. Data for the 2012 scan. The c.m. energy ($\sqrt{s}$), integrated luminosity (L), number of selected $e^+e^- \to K^+K^-$ events ($N_{\rm exp}$), detection efficiency (ε_0), radiative correction factor ($1+\delta$), and $e^+e^- \to K^+K^-$ Born cross section (σ_0). For number of events, only the statistical uncertainty is quoted. For the cross section, the first error is statistical, the second is systematic. The value in parentheses is a part of the systematic uncertainty associated with background subtraction.

$\sqrt{s}$, GeV	L, nb^{-1}	$N_{\rm exp}$	ε_0	$1+\delta$	σ_0, nb
1.277	763	2795 ± 62	0.653	0.882	$6.358 \pm 0.142 \pm 0.105(0.027)$
1.357	845	2676 ± 61	0.670	0.886	$5.339 \pm 0.122 \pm 0.089(0.023)$
1.435	1032	2556 ± 61	0.675	0.892	$4.114 \pm 0.099 \pm 0.069(0.020)$
1.515	940	2031 ± 54	0.678	0.891	$3.574 \pm 0.094 \pm 0.060(0.018)$
1.595	822	1604 ± 44	0.666	0.888	$3.302 \pm 0.090 \pm 0.055(0.016)$
1.674	914	1044 ± 36	0.682	0.944	$1.770 \pm 0.062 \pm 0.031(0.013)$
1.716	512	373 ± 25	0.673	0.967	$1.115 \pm 0.075 \pm 0.025(0.018)$
1.758	804	282 ± 21	0.658	1.068	$0.503 \pm 0.038 \pm 0.014(0.012)$
1.798	1012	136 ± 18	0.683	1.069	$0.187 \pm 0.025 \pm 0.016(0.015)$
1.840	568	103 ± 15	0.676	0.915	$0.293 \pm 0.041 \pm 0.014(0.013)$
1.874	936	152 ± 18	0.675	0.870	$0.276 \pm 0.033 \pm 0.016(0.015)$
1.903	962	162 ± 18	0.677	0.867	$0.287 \pm 0.033 \pm 0.017(0.016)$
1.926	680	148 ± 18	0.679	0.872	$0.367 \pm 0.044 \pm 0.016(0.014)$
1.945	929	145 ± 19	0.676	0.876	$0.263 \pm 0.034 \pm 0.015(0.014)$
1.967	755	147 ± 18	0.666	0.885	$0.331 \pm 0.041 \pm 0.015(0.014)$
1.989	641	131 ± 17	0.666	0.889	$0.346 \pm 0.046 \pm 0.015(0.014)$

which is inverted to suppress events with kaons: $(dE/dx)_1 + (dE/dx)_2 < 2(dE/dx)_e$. Events of the $e^+e^- \to e^+e^-$ process are suppressed by the requirement $E_{\rm tot}/\sqrt{s} < 0.7$, while $e^+e^- \to \mu^+\mu^-$ and cosmic background is rejected by the muon-system veto and the condition that the energy deposition in the upper half of the calorimeter is outside the range of the peak from minimum-ionizing particles. The number of selected $e^+e^- \to \pi^+\pi^-$ events coincides with the number expected from simulation within 10%. This value is taken as an estimate of the systematic uncertainty on the pion background calculation.

To determine the number of kaon events, the $E_{\rm tot}/\sqrt{s}$ distribution is fitted by a sum of muon, kaon, and electron distributions. The distributions for background processes are obtained from data. A practically pure sample of $e^+e^- \to e^+e^-$ events is selected by the requirement that one of the particles in an event passes through the ACC active area and produces a Cherenkov signal. The muon distribution is obtained using events selected with the requirement that the muon system fires. The $E_{\rm tot}/\sqrt{s}$ distribution for such events is shown in Fig. 3. It is seen that the muon peak survives, while kaon and electron events are strongly suppressed. To study the distribution for cosmic muons, the condition on the parameters d_i is modified: $0.25 < |d_{1,2}| < 0.5$. This allows us to reject e^+e^- annihilation events and obtain a pure spectrum of cosmic muons. It is found that the muon distribution consist of two components. One of the components, with higher energy deposition, contains $e^+e^- \to \mu^+\mu^-$ events and events with energetic cosmic muons. The other component contains cosmic muons with momentum less than the threshold momentum for muons in ACC. This second component is seen in Fig. 4, which shows the $E_{\rm tot}/\sqrt{s}$ distribution for events, in which the condition of no ACC signal is applied to both particles.

The kaon distribution is obtained using simulation. To take into account a possible inaccuracy in simulation of detector response, the distribution is convolved with a Gaussian distribution, the parameters which (a shift of the peak position δx and sigma σ_x, where $x \equiv E_{\rm tot}/\sqrt{s}$) are determined from the fit to data. The fit results for events from the energy range $\sqrt{s} = 1.4$–1.6 selected with different conditions are shown in Figs. 2, 3, and 4. It is seen that the fitted curves describe data well. For this range, the parameters δx and σ_x are found to be -0.019 ± 0.002 and 0.034 ± 0.006, respectively.

The fitted numbers of kaon events with subtracted $e^+e^- \to \pi^+\pi^-$ contribution are listed in Tables I and II for the 2011 and 2012 scans, respectively.

V. DETECTION EFFICIENCY

The detection efficiency for the process under study is determined using MC simulation. The simulation takes into account extra photon radiation from the initial state [17,18]. The detection efficiency (ε) is calculated as a function of $\sqrt{s}$ and the energy of the photon (E_γ) emitted by the initial particles. The energy dependence of the detection efficiency for $e^+e^- \to K^+K^-$ events with $E_\gamma = 0$ is shown in Fig. 5. The decrease of the efficiency when the energy approaches the reaction threshold is explained by an increase of the fraction of events with a kaon decayed before ACC. A nonmonotonic behavior of the detection efficiency as a function of energy is due to variation of experimental

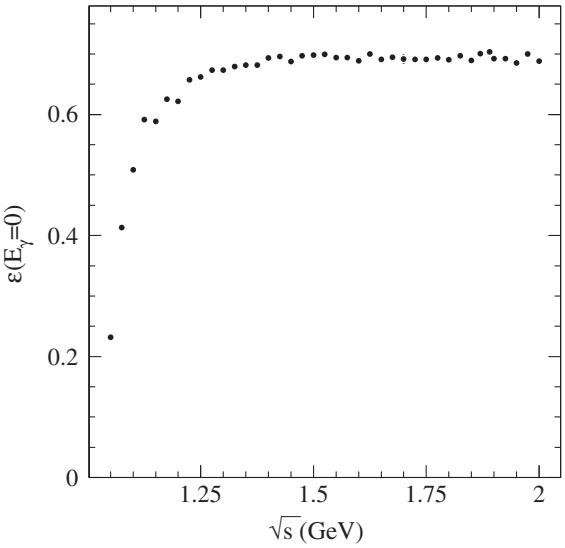

FIG. 5. The energy dependence of the detection efficiency for $e^+e^- \to K^+K^-$ events with $E_\gamma = 0$.

conditions during data taking, in particular, the number of dead detector channels and the level of beam background. A typical dependence of the detection efficiency on E_γ is shown in Fig. 6.

The efficiency determined from MC simulation is corrected to take into account a difference between data and simulation in detector response and the absence of the final state radiation (FSR) in the $e^+e^- \to K^+K^-$ simulation. Corrections associated with inaccuracy of detector simulation is described by three correction factors: for kinematic selection criteria ($c_{\rm kin}$), e.g., the conditions on $\Delta\theta$ and $\Delta\phi$, for the geometric condition that one of the particles

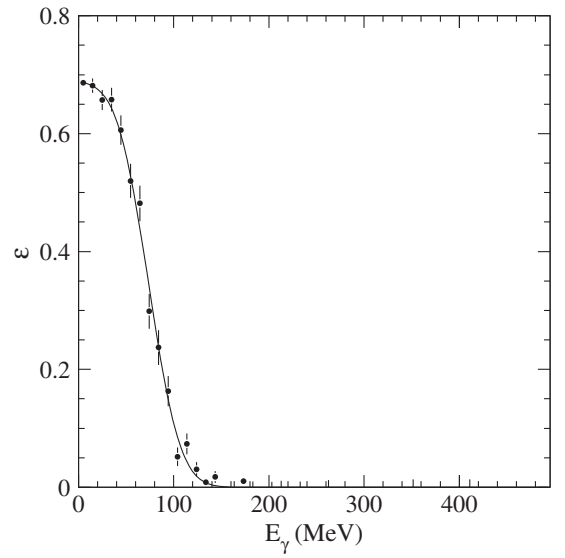

FIG. 6. The dependence of the detection efficiency on the energy of the photon emitted from the initial state at $\sqrt{s} = 1.6$ GeV.

must pass through the active ACC area ($c_{\rm geo}$), and for the kaon identification condition ($c_{\rm id}$). To measure the corrections of the first group, the condition on the parameter under study is loosened. Tighter conditions may be applied on other kinematic parameters. The correction factor is calculated as follows:

$$c_i = \frac{n/n'}{m/m'}, \tag{1}$$

where n and m are the numbers of events in data and simulation obtained with the standard condition on the parameter under study, and n' and m' are the same numbers with a looser condition. The total correction factor for the kinematic conditions is calculated as a product of the factors obtained for each of the condition and is found to be $c_{\rm kin} = 1.008 \pm 0.002$.

The identification correction is determined as follows. The cross section for $e^+e^- \to K^+K^-$ is measured for two sets of selection criteria. In the first set, it is required that both particles pass through the active ACC area, but only one of them is identified as a kaon (no signal in ACC). In the second set, it is required that both particles pass through the active ACC area and are identified as kaons. Since the geometric conditions are identical in the both selections, the ratio of the cross sections is equal to the value of the identification correction factor. It is found that $c_{\rm id}$ is independent of energy and is equal to 1.003 ± 0.007 for the 2011 scan and 1.004 ± 0.012 for the 2012 scan. The closeness of the obtained correction factors to unity indicates that our simulation reproduces the ACC response for kaons well.

The geometric correction is estimated using $e^+e^- \to e^+e^-$ events. The fractions of events, in which one of the particle tracks extrapolates to the ACC active area, are determined in data and simulation. From their ratio, the geometric correction factor is obtained to be $c_{\rm geo} = 1.0017 \pm 0.0004$ for the 2011 scan and $c_{\rm geo} = 0.9974 \pm 0.0007$ for the 2012 scan.

As was mentioned above, our signal simulation does not include FSR and therefore, reproduces the $\Delta\theta$ and $\Delta\phi$ distributions incorrectly. In particular, some fraction of FSR events falls into the corner regions of the two-dimensional $\Delta\phi$ vs $\Delta\theta$ distribution in Fig. 1, which are used to estimate the noncollinear background. The effect of FSR on the detection efficiency is studied with the event generator based on Ref. [19], which includes both initial and final state radiation. Using MC simulation at the generator level, the detection efficiencies calculated with and without FSR are compared. The inclusion of FSR reduces the efficiency by 0.1% at 1.1 GeV, 0.7% at 1.5 GeV, and 1.3% at 2.0 GeV.

The corrected values of the detection efficiency $\varepsilon_0 \equiv \varepsilon(E_\gamma = 0)$ are listed in Tables I and II for 2011 and 2012, respectively. The uncertainty of the total correction factor is 0.7% for 2011 and 1.2% for 2012. These values are taken as an estimate of the systematic uncertainties on the detection efficiency.

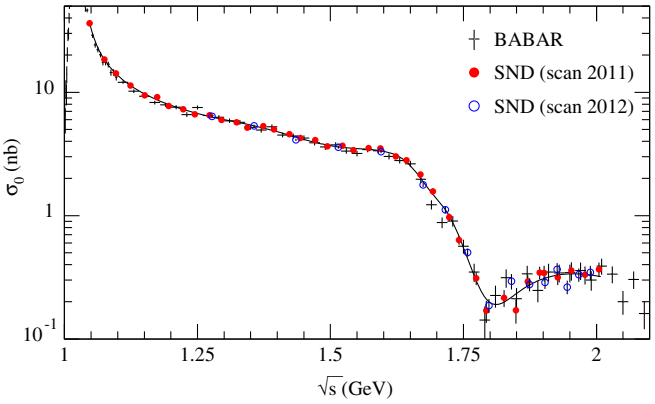

FIG. 7. The Born cross section for the process $e^+e^- \to K^+K^-$ measured in this work and in the *BABAR* experiment [12]. The curve is the result of the fit described in the text.

VI. BORN CROSS SECTION

The experimentally observed cross section of the process under study $\sigma_{\rm vis}$ is related to the Born cross section σ_0 by the formula

$$\sigma_{\rm vis}(\sqrt{s}) = \int_0^{z_{\rm max}} dz \sigma_0(\sqrt{s(1-z)}) F(z,s) \varepsilon(\sqrt{s},z), \qquad (2)$$

where $F(z,s)$ is a function describing the probability to emit extra photons with the total energy $z\sqrt{s}/2$ from the initial state [17], $\varepsilon(\sqrt{s},z)$ is the detection efficiency, and $z_{\rm max} = 1 - 4m_K^2/s$. The following procedure is used to determine the experimental values of the Born cross section. The measured cross section $\sigma_{{\rm vis},i} = N_{{\rm exp},i}/L_i$, where $N_{{\rm exp},i}$ is the number of selected events with subtracted background and L_i is the integrated luminosity for ith energy point, is fitted by Eq. (2) with a theoretical model for the Born cross section. As a result of the fit, parameters of the model are determined, and the radiation correction factor is calculated as $1 + \delta(s) = \sigma_{\rm vis}(s)/(\varepsilon_0(s)\sigma_0(s))$, where $\varepsilon_0(s) \equiv \varepsilon(s, z = 0)$. The experimental values of the Born cross sections are then obtained as

$$\sigma_{0,i} = \frac{\sigma_{{\rm vis},i}}{\varepsilon_0(s_i)(1+\delta(s_i))}. \qquad (3)$$

The vector meson dominance model is used to describe the Born $e^+e^- \to K^+K^-$ cross section [20]

$$\sigma_0(s) = \frac{\pi\alpha^2\beta^3}{3s}|F_K(s)|^2(1+C_{\rm FS}), \qquad (4)$$

$$F_K(s) = \sum_{V=\rho,\omega,\phi,\ldots} a_V e^{i\phi_V} \frac{m_V^2}{m_V^2 - s - i m_V \Gamma_V(s)}, \qquad (5)$$

where α is the fine structure constant, $\beta = \sqrt{1-4m_K^2/s}$, $C_{\rm FS}$ is a factor describing radiation corrections to the final state [21], which varies from about 3% at $\sqrt{s} = 1.05$ GeV to 0.9% at $\sqrt{s} = 2.0$ GeV. The charged kaon electromagnetic form factor $F_K(s)$ is a sum of the contributions of the ρ, ω, and ϕ resonances and their excited states. The masses (m_V), widths (Γ_V), amplitudes (a_V), and the relative phases (ϕ_V) of the ρ, ω, and ϕ are fixed using Particle Data Group (PDG) data [22] and SU(3) relations. For the masses and widths of excited states, PDG values are taken, while their amplitudes and phases are free fit parameters. The energy-dependent widths of the ρ, ω, and ϕ resonances take into account decays with branching fractions larger than 1%. For exited states, the $\Gamma(s)$ is described by a simpler model including only the p-wave decay into K^+K^-. The model describes data reasonably well ($\chi^2/ndf = 65/46$). The fit result is shown in Fig. 7. The values of the Born cross section calculated using Eq. (3) together with the values of the radiation correction factors are listed in Tables I and II.

VII. SYSTEMATIC ERRORS

The sources of systematic uncertainties on the measured cross section are listed in Table III.

The integrated luminosity is measured on events of the processes $e^+e^- \to e^+e^-$ and $e^+e^- \to \gamma\gamma$, the cross sections for which are known with an accuracy better than 1%. The relative difference between these two measurements is independent of the c.m. energy and does not exceed 1%. This value is taken as an estimate of the systematic uncertainty on the luminosity measurement.

The uncertainty on the detection efficiency is discussed in Sec. V. The systematic uncertainties associated with

TABLE III. The average over the energy intervals systematic uncertainties (%) on the measured $e^+e^- \to K^+K^-$ cross section.

	2011		2012	
source	$\sqrt{s} < 1.8$ GeV	$\sqrt{s} > 1.8$ GeV	$\sqrt{s} < 1.8$ GeV	$\sqrt{s} > 1.8$ GeV
Luminosity	1.0	1.0	1.0	1.0
Detection efficiency	0.7	0.7	1.2	1.2
Background subtraction	0.7	4.1	0.7	4.1
Nuclear interaction	0.1	0.1	0.1	0.1
Radiative correction	0.1	0.1	0.1	0.1
Total	1.4	4.3	1.7	4.4

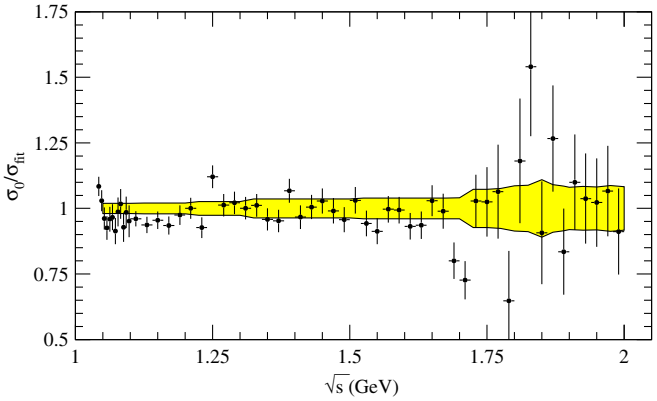

FIG. 8. The relative difference between the $e^+e^- \to K^+K^-$ cross section measured in the *BABAR* experiment [12] and the fit to SND data shown in Fig. 7. For *BABAR* data (points with error bars), the statistical errors (diagonal elements of the covariance matrix) are shown. The shaded band represents the SND and *BABAR* systematic uncertainties combined in quadrature. The *BABAR* systematic uncertainty is 1.49% at $\sqrt{s} = 1.05$–1.10 GeV, 1.64% at $\sqrt{s} = 1.1$–1.2 GeV, 2.23% at $\sqrt{s} = 1.2$–1.3 GeV, 3.37% at $\sqrt{s} = 1.3$–1.5 GeV, 3.73% at $\sqrt{s} = 1.5$–1.7 GeV, and 7.03% above 1.7 GeV.

the subtraction of the noncollinear and $e^+e^- \to \pi^+\pi^-$ backgrounds are discussed in Sec. IV. Accuracy of the subtraction of the muon and electron backgrounds in the fit to the $E_{\rm tot}/\sqrt{s}$ distribution is tested by the comparison of the cross sections measured on events with one and two identified kaons. The ratio of the cross sections is described by the coefficient $c_{\rm id}$. Since both electron and muon contributions to the $E_{\rm tot}/\sqrt{s}$ spectra with these two selections are strongly different (see Figs. 2 and 4) and the $c_{\rm id}$ value is consistent with unity, we do not introduce an additional systematic uncertainty associated with the fit to the $E_{\rm tot}/\sqrt{s}$ distribution.

A part of kaon events is lost due to the kaon nuclear interaction in the material before the drift chamber. Its thickness is about 0.5% of the nuclear interaction length. Taking into account that the cross sections for the charged kaon nuclear interactions are well known, we estimate that the systematic uncertainty associated with the kaon nuclear interaction does not exceed 0.1%. The theoretical uncertainty on the radiative correction calculation is less than 0.1% [17].

We assume that all the sources of systematic uncertainties are independent and add them in quadrature. The resulting total systematic uncertainty is listed in Table III.

VIII. SUMMARY

In this paper, the $e^+e^- \to K^+K^-$ cross section has been measured in the c.m. energy range 1.05–2.00 GeV. The data with an integrated luminosity of 34.6 pb^{-1} collected with the SND detector at the VEPP-2000 e^+e^- collider VEPP-2000 in 2011 and 2012 have been used for this measurement. The obtained cross section has a complex energy dependence (see. Fig. 7) explained by the fact that all resonances of the ρ, ω, and ϕ families give contributions to the $e^+e^- \to K^+K^-$ amplitude.

The comparison of our measurement with the most accurate previous measurement of the $e^+e^- \to K^+K^-$ cross section in the *BABAR* experiment [12] is shown in Figs. 7 and 8. Our measurement is in good agreement with *BABAR* data and has comparable or better accuracy. We confirm the disagreement with the SND@VEPP-2M [1] and DM2 [11] $e^+e^- \to K^+K^-$ data observed by *BABAR*. The previous SND measurement [1] was performed with the detector not having a special particle identification system. The kaon separation from pions, muons, and electrons was based mainly on information about particle energy depositions in the calorimeter. The complex procedure was used to determine identification efficiencies from data. Currently, we think, that the systematic uncertainty in the SND@VEPP-2M measurement [1] was underestimated.

ACKNOWLEDGMENTS

This work is supported in part by the RFBR Grants No. 16-02-00327-a, No. 16-02-00014-a, and No. 15-02-01037.

[1] M. N. Achasov *et al.* (SND Collaboration), Phys. Rev. D **76**, 072012 (2007).
[2] M. N. Achasov *et al.* (SND Collaboration), J. Exp. Theor. Phys. **103**, 720 (2006).
[3] M. N. Achasov *et al.* (SND Collaboration), J. Instrum. **10**, P09006 (2015).
[4] M. N. Achasov *et al.*, Nucl. Instrum. Methods Phys. Res., Sect. A **598**, 31 (2009).
[5] V. M. Aulchenko *et al.*, Nucl. Instrum. Methods Phys. Res., Sect. A **598**, 102 (2009).
[6] A. Y. Barnyakov *et al.*, J. Instrum. **9**, C09023 (2014); A. Y. Barnyakov *et al.*Instrum. Exp. Tech. **58**, 30 (2015).

[7] V. M. Aulchenko *et al.*, Nucl. Instrum. Methods Phys. Res., Sect. A **598**, 340 (2009).
[8] A. Romanov *et al.*, in *Proceedings of PAC 2013, Pasadena, CA USA*, p. 14, http://accelconf.web.cern.ch/AccelConf/PAC2013/papers/mooaa2.pdf.
[9] P. M. Ivanov, L. M. Kurdadze, M. Yu. Lelchuk V. A. Sidorov, A. N. Skrinsky, A. G. Chilingarov, Yu. M. Shatunov, B. A. Shwartz, and S. I. Eidelman (OLYA Collaboration), Phys. Lett. B **107B**, 297 (1981).
[10] B. Delcourt, D. Bisello, J.-C. Bizot, J. Buon, A. Cordier, and F. Mané (DM1 Collaboration) Phys. Lett. B **99B**, 257 (1981).
[11] D. Bisello *et al.* (DM2 Collaboration), Z. Phys. C **39**, 13 (1988).
[12] J. P. Lees *et al.* (*BABAR* Collaboration), Phys. Rev. D **88**, 032013 (2013).
[13] E. V. Abakumova *et al.*, Nucl. Instrum. Methods Phys. Res., Sect. A **744**, 35 (2014); E. V. Abakumova, M. N. Achasov, A. A. Krasnov, N. Yu. Muchnoi, and E. E. Pyata, J. Instrum. **10**, T09001 (2015).
[14] R. R. Akhmetshin *et al.* (CMD-3 Collaboration), Phys. Lett. B **759**, 634 (2016).
[15] D. N. Shemyakin *et al.* (CMD-3 Collaboration), Phys. Lett. B **756**, 153 (2016).
[16] B. Aubert *et al.* (*BABAR* Collaboration), Phys. Rev. Lett. **103**, 231801 (2009).
[17] E. A. Kuraev and V. S. Fadin, Yad. Fiz. **41**, 733 (1985) [Sov. J. Nucl. Phys. **41**, 466 (1985)].
[18] G. Bonneau and F. Martin, Nucl. Phys. **B27**, 381 (1971).
[19] A. B. Arbuzov, E. A. Kuraev, V. A. Astakhov, G. V. Fedotovich, A. V. Fedorov, and N. P. Merenkov, J. High Energy Phys. 10 (1997) 006.
[20] C. Bruch, A. Khodjamirian, and J. H. Kuhn, Eur. Phys. J. C **39**, 41 (2005).
[21] A. Hoefer, J. Gluza, and F. Jegerlehner, Eur. Phys. J. C **24**, 51 (2002).
[22] K. A. Olive *et al.* (Particle Data Group), Chin. Phys. C **38**, 090001 (2014).